Tracing Long-Lived Atomic Coherences Generated via Molecular Conical Intersections

Patrick Rupprecht,[1,2,*,†] Francesco Montorsi,[3,*,‡] Lei Xu,[4] Nicolette G. Puskar,[1,2] Marco Garavelli,[3] Shaul Mukamel,[5] Niranjan Govind,[4,6] Daniel M. Neumark,[1,2,§] Daniel Keefer,[7,‖] and Stephen R. Leone[1,2,8,¶]

[1]*Department of Chemistry, University of California, Berkeley, California 94720, USA*
[2]*Chemical Sciences Division, Lawrence Berkeley National Laboratory, Berkeley, California 94720, USA*
[3]*Università di Bologna—Alma Mater Studiorum, Via Piero Gobetti 85, 40129 Bologna, Italy*
[4]*Physical and Computational Sciences Directorate, Pacific Northwest National Laboratory, Richland, Washington 99352, USA*
[5]*Department of Chemistry and Department of Physics and Astronomy, University of California, Irvine, California 92697-2025, USA*
[6]*Department of Chemistry, University of Washington, Seattle, Washington 98195, USA*
[7]*Max Planck Institute for Polymer Research, Mainz 55128, Germany*
[8]*Department of Physics, University of California, Berkeley, California 94720, USA*

(Received 8 April 2025; accepted 16 October 2025; published 5 December 2025)

Accessing coherences is key to fully understand and control ultrafast dynamics of complex quantum systems like molecules. Most photochemical processes are mediated by conical intersections, which generate coherences between electronic states in molecules. We show with accurate calculations performed on gas-phase methyl iodide that electronic coherences of spin-orbit-split states persist in atomic iodine after dissociation. Our simulation predicts a maximum magnitude of vibronic coherence in the molecular regime of 0.75% of the initially photoexcited state population. Upon dissociation, one-third of this coherence magnitude is transferred to a long-lived atomic coherence where vibrational decoherence can no longer occur. To trace these dynamics, we propose a tabletop experimental approach—heterodyned attosecond four-wave-mixing spectroscopy. This technique can temporally resolve small electronic coherence magnitudes and reconstruct the full complex coherence function via phase cycling. Hence, heterodyned attosecond four-wave-mixing spectroscopy leads the way to a complete understanding and optimal control of spin-orbit-coupled electronic states in photochemistry.

DOI: 10.1103/6bfk-mgpn

In the evolution of quantum systems, the population of specific quantum states is relevant as well as the distinct phase relation between them. This phase relation or quantum coherence has broad applications in physics [1] and chemistry [2] and is key for cutting-edge applications like quantum computing [3]. Coherence between excited electronic states in molecules can be initiated externally through interaction with an ultrafast laser pulse [4–6] or internally via coupled electron-nuclear dynamics on the femtosecond timescale [7]. The latter case is facilitated by wave-packet (WP) splitting at conical intersections (CIs). These are singular regions of the potential energy surface (PES) where at least two electronic states are energetically degenerate. CIs are crucial for most photochemical reactions [8–15]. At CIs, the initial WP branches into the two intersecting electronic states. As both resulting WPs originate from the same initial state, they can exhibit a significant degree of coherence depending on the molecular symmetry [16]. Moreover, since electronic and nuclear dynamics around CIs are strongly coupled, the resulting coherence in the molecule is refereed to as *vibronic* coherence. The temporal evolution of the vibronic coherence and its vanishing due to intramolecular vibrations are important components for a complete understanding and potential control of nonadiabatic molecular dynamics. It is challenging, however, to directly link measurement signatures to vibronic coherence via standard experimental schemes such as attosecond x-ray transient-absorption spectroscopy [17]. In recent years, multiple alternative experimental approaches have been proposed and theoretically discussed [18,19], one notably labeled TRUECARS [20]. These approaches require large-scale user facilities, such as x-ray free-electron lasers [21] or ultrafast electron diffraction [22] setups.

*These authors contributed equally to this work.
†Contact author: prupprecht@lbl.gov
‡Contact author: francesco.montorsi4@unibo.it
§Contact author: dneumark@berkeley.edu
‖Contact author: keeferd@mpip-mainz.mpg.de
¶Contact author: srl@berkeley.edu

Published by the American Physical Society under the terms of the Creative Commons Attribution 4.0 International license. Further distribution of this work must maintain attribution to the author(s) and the published article's title, journal citation, and DOI. Open access publication funded by the Max Planck Society.

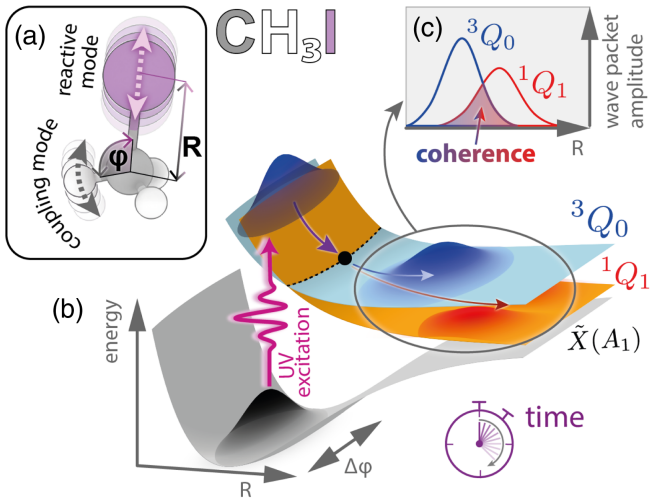

FIG. 1. Electronic coherence in the photodynamics of CH_3I. (a) Molecular structure of CH_3I with the indicated reactive vibrational mode R (C—I bond length) and coupling vibrational mode φ (H—C—I bending angle) used to model the PESs. (b) Photodynamics along the respective PESs: a WP is excited from the $\tilde{X}(A_1)$ ground state to the $^3Q_0$ excited-state PES via a UV pulse. After some time, the WP reaches the CI region (dotted line and black dot) where a part of the WP is transferred to the $^1Q_1$ PES. (c) After further propagation, the coherence is determined via the wave-function overlap of both WPs.

In this Letter, we theoretically investigate the vibronic coherence evolution in gas-phase CH_3I molecules after excitation with an ultraviolet (UV) pulse. Here, the initial photoexcited WP bifurcates at a CI to propagate on two dissociative PESs, which ultimately results in a ground-state or a spin-orbit-excited iodine fragment. Surprisingly, one-third of the maximum coherence magnitude spawned at the molecular CI is maintained in the atomic limit where no vibrational decoherence can occur. In order to trace the evolution of electronic coherence from the molecular to the atomic regime, we propose and model a novel tabletop experimental technique: heterodyned attosecond four-wave-mixing spectroscopy (Hd-FWM). Theoretical benchmarking of the anticipated Hd-FWM signal demonstrates its direct sensitivity to weak coherences and its capability to monitor the complete complex coherence function.

Photoinduced bond cleavage in CH_3I [along R coordinate in Fig. 1(a)] is a paradigm for photodissociation in polyatomic molecules. Consequently, this system has been the subject of extensive experimental [23–29] and theoretical [30–33] studies. UV excitation around 260 nm triggers $I(5p) \rightarrow \sigma^*$ electronic transitions in CH_3I, which result in the $^3Q_0$ and $^1Q_1$ spin-orbit-split states [34,35]. Both display steep dissociative PESs as illustrated in Fig. 1(b) that lead to the $j = \{1/2, 3/2\}$ states of the atomic iodine fragment. Laser excitation initiates the dynamics predominantly on the $^3Q_0$ PES [28,32], which is accessed via a one-UV-photon transition from the $\tilde{X}(A_1)$ ground state. During dissociation, a $^3Q_0/^1Q_1$ CI is encountered after about 15 fs [28]. This results in the generation of a vibronic coherence that is determined by the $^3Q_0/^1Q_1$ WP overlap $\langle \chi_{^3Q_0}(t) | \chi_{^1Q_1}(t) \rangle$ [see Fig. 1(c)].

We model this phenomenon using exact nuclear quantum dynamics (QD) in reduced dimensions as implemented in the QDng software [36,37]. In particular, we employ an effective two-dimensional Hamiltonian comprising the diabatic $^3Q_0$ and $^1Q_1$ states, which reproduces the results of the full nine-dimensional *ab initio* model previously reported by Amatatsu, Yabushita, and Morokuma [30] and further corrected by Xie *et al.* [31]. The two nuclear degrees of freedom spanning the system Hamiltonian were chosen to encompass a large cross section of the $^3Q_0/^1Q_1$ branching space. As illustrated in Fig. 1(a), these coordinates are the symmetry-preserving (*reactive*) C—I stretching (R) and the symmetry-breaking (*coupling*) H—C—I bending (φ). This QD setup provides population dynamics and $j = \{1/2, 3/2\}$ branching ratios (Fig. S2 in Supplemental Material [38]) in good agreement with previous theoretical studies [32,33]. Hence, other CH_3I vibrational modes do not significantly influence the photodissociation dynamics.

The vibronic coherence established at the CI is probed by spectroscopically targeting the $4d \rightarrow 5p$ core-to-valence transition of iodine [54]. This results in a pair of spin-orbit-split core-excited states, $\sigma^*(4d_{5/2})^{-1}$ and $\sigma^*(4d_{3/2})^{-1}$. These states are computed by many-body all-electron quantum chemistry (QC) calculations using the multireference configuration interaction [55,56] method including spin-orbit coupling effects as implemented in the MOLPRO [57] package. More details about the QC simulations are given in Supplemental Material Sec. III [38].

We propose the Hd-FWM technique for directly measuring the electronic coherence evolution in CH_3I in a time-resolved manner. Noncollinear attosecond FWM spectroscopy is a well-established tabletop experimental approach that targets the $\chi^{(3)}$ nonlinear response of highly excited states in atoms [58–64], molecules [65–67], and solid-state systems [68] by mixing a broadband XUV pulse with two few-cycle near-infrared (NIR) or visible (VIS) pulses. The attosecond XUV pulse is produced via high-order harmonic generation [69–71] and shares the same driving laser as the NIR and VIS pulses, hence enabling precise timing and control over the pulse characteristics. So far, attosecond FWM spectroscopy has been used to measure lifetimes of highly excited states in a quantum-state-specific manner [62,64] as well as to characterize electronic and vibrational coherences in atoms and molecules [63,65,72].

The novelty of the proposed approach consists of interfering two FWM signals, which enhances the sensitivity such that this technique can unambiguously measure small vibronic coherence magnitudes in molecules. Figure 2 shows the general experimental scheme: The ultrashort UV pump pulse centered at 260 nm photoexcites CH_3I. Four pulses then act at a variable time delay and

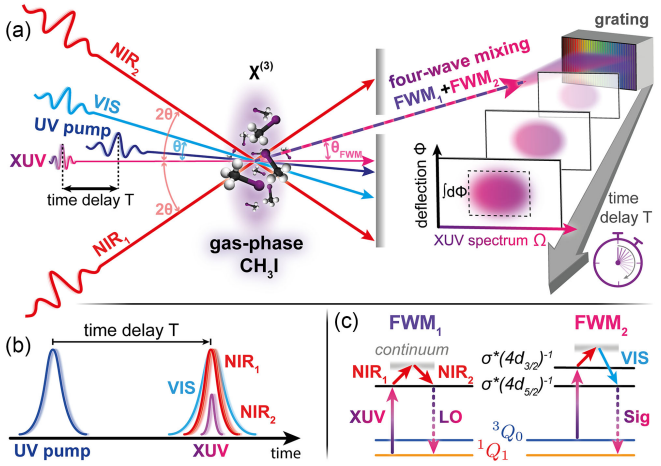

FIG. 2. Heterodyned attosecond four-wave-mixing spectroscopic scheme. (a) After photoexcitation via the UV pump pulse, four time-delayed pulses interact with gas-phase CH_3I. First, the broadband XUV pulse, the NIR_1, and the NIR_2 pulses result in the FWM_1 signal via a $\chi^{(3)}$ process. Additionally, the XUV, NIR_1, and VIS pulses result in the FWM_2 signal. By choosing the correct noncollinear geometry, FWM_1 and FWM_2 overlap spectrally and spatially on a CCD chip of the XUV spectrograph. (b) The measurement variable is the time delay between the UV and all other pulses. (c) Hd-FWM quantum pathways: NIR_1 and NIR_2 couple to the continuum in a Raman process and result in a degenerate FWM_1 emission, which acts as local oscillator (LO). FWM_2 utilizes a Raman process via NIR_1 and the VIS pulse to result in the coherence-encoding signal (Sig).

contribute to the FWM signals: A broadband XUV pulse interacts with NIR_1 and NIR_2 ($\lambda_{NIR} = 800$ nm) in the gas-phase CH_3I sample resulting in the FWM_1 signal. Because of the noncollinear beam geometry (XUV-NIR angle $\pm 2\Theta$) and the Λ-coupling scheme [see Fig. 2(c)], FWM_1 propagates with a noncollinear angle Θ_{FWM} with respect to the XUV input beam in accordance with the phase-matching condition. This resulting noncollinear emission angle Θ_{FWM} enables the spatial separation from the transmitted input pulses. The second signal FWM_2 results from the interaction of XUV, NIR_1, and a pulse at the second harmonic of 800 nm (VIS; $\lambda_{VIS} = 400$ nm). By choosing the XUV-VIS angle to be Θ, FWM_1 and FWM_2 share the same noncollinear angle and, hence, are spatially overlapped at the spectrograph. Spectral overlap with FWM_1 is evident by the respective coupling pathway of FWM_2 in Fig. 2(c): The XUV-emission transition is in both cases $\sigma^*(4d_{5/2})^{-1} \rightarrow {}^1Q_1$. While FWM_1 projects the population of the ${}^1Q_1$ PES onto itself via coupling to the $\sigma^*(4d_{5/2})^{-1}$ core-excited PES and acts as a reference field (local oscillator; LO), FWM_2 couples the ${}^3Q_0$ and ${}^1Q_1$ PESs and, hence, encodes the desired coherence signal (Sig).

The total intensity I_T detected by the XUV spectrograph at Θ_{FWM} as a function of the time delay T results from the superposition of the LO (E_{LO}) and signal (E_S) electric fields [73]:

$$I_T(T,\Omega) \propto I_{LO}(T,\Omega) + I_S(T,\Omega) + 2\mathrm{Re}[E^*_{LO}(T,\Omega)E_S(T,\Omega)]. \quad (1)$$

Here, I_{LO} and I_S are the intensities of the LO and signal components, respectively (i.e., $|E_{LO}|^2$ and $|E_S|^2$), while Ω is the FWM emission photon energy. The LO is directly sensitive to the ${}^1Q_1$ population while the signal detects the much weaker electronic coherence. This results in $E_{LO} \gg E_S$. Therefore, the I_S term in Eq. (1) can be neglected. Moreover, I_{LO} is easily measured by blocking the VIS pulse. Consequently, by subtracting I_{LO} from I_T, the FWM interference is isolated, yielding the Hd-FWM measured intensity signal

$$I_{Hd}(T,\Omega) \propto 2\mathrm{Re}[E^*_{LO}(T,\Omega)E_S(T,\Omega)]. \quad (2)$$

Both E_{LO} and E_S are evaluated here using third-order perturbation theory. That is achieved by expanding the FWM_1 and FWM_2 response functions as a series of Feynman diagrams [73], each corresponding to a specific quantum pathway connecting valence and core excited states (see Fig. S5 in Supplemental Material [38]). This rationalizes the Hd-FWM process as the interference between two dominating coupling pathways as depicted in Fig. 2(c). Other possible third-order coupling pathways are not phase-matched at Θ_{FWM}, emit at a different XUV photon energy, or are negligible due to transition-dipole-moment considerations [26]. A detailed discussion about the third-order coupling pathways is given in Supplemental Material Sec. IV b [38]. Further higher-order pathways that might be phase-matched can be safely neglected by lowering the intensities of the NIR and VIS pulses such that the FWM signal is just measurable within the necessary signal-to-noise ratio [73].

The Hd-FWM simulation results in the $I_T(T,\Omega)$ spectrogram displayed in Fig. 3(a). We observe an oscillating feature in the spectral region between 45.5 and 46.5 eV, which rises at around 15 fs, at the conical intersection. Here, the $\chi_{^3Q_0}$ WP splits leading to the simultaneous occurrence of both FWM_1 and FWM_2, which is required to observe the Hd-FWM signal. Moreover, the centroid of the signal displays a transient blueshift tracking the increasing $\sigma^*(4d_{5/2})^{-1} - {}^1Q_1$ energy gap during the dynamics [black dashed line in Fig. 3(a)]. Such behavior can be understood by benchmarking valence against core-excited-state PESs (see Supplemental Material, Fig. S4 [38]). If the relative carrier-envelope phase (CEP) between the NIR_2 and VIS pulses is zero, the intensity oscillation recorded in the Hd-FWM signal matches the real part [see Fig. 3(b)] of the coherence spawned at the molecular CI, therefore providing a direct measure of the coherence evolution [see Fig. 3(c)]. Alternatively, if the relative CEP is set to $\pi/2$, the Hd-FWM maps the imaginary part of the coherence [see Fig. 3(d)]. This demonstrates that

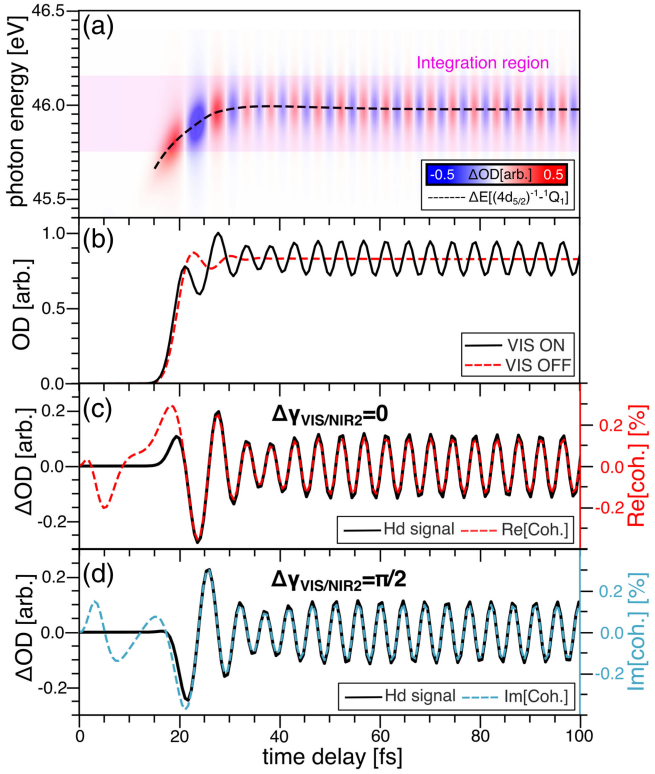

FIG. 3. Simulated Hd-FWM electronic coherence signal. (a) Hd-FWM spectrogram as a function of the FWM emission energy Ω and *pump-probe* time delay T. The black dashed line depicts the time evolution of the $\sigma^*(4d_{5/2})^{-1} - {}^1Q_1$ energy gap during the dynamics. (b) Simulated FWM trace with [$I_T(T,\Omega)$; black solid line] and without [$I_{\mathrm{LO}}(T,\Omega)$; red dashed line] the VIS pulse highlighting the formation of FWM interference. (c) Oscillating component $I_{\mathrm{Hd}}(T,\Omega)$ of (b) matching the real part of the electronic coherence (red dashed line). (d) The same as (c) but applying a relative CEP offset of $\pi/2$ between the VIS and the NIR_2 pulses. Now, the Hd signal traces the imaginary part of the coherence (dashed light-blue line) granting access to the full complex coherence function. Traces (b)–(d) are obtained by integrating the signal in the photon-energy window displayed in (a).

Hd-FWM uniquely provides access to the complete complex coherence by probing separately its real and imaginary parts via a phase-cycling approach known from other multidimensional spectroscopy schemes [74]. As XUV and NIR_1 pulses are simultaneously involved in both FWM_1 and FWM_2, their CEPs are not cycled, since they do not affect the relative phase between the E_{LO} and the E_{S} field.

Notably, the anticipated vibronic coherence magnitude in CH_3I is minimal, i.e., about 0.75% of the photoexcited initial ${}^3Q_0$ state population. This is a consequence of the different symmetries of ${}^1Q_1$ and ${}^3Q_0$ that respectively belong to the $E(A')$ and A_1 irreducible representations of the C_{3v} point group [32]. As previously found by Neville, Stolow, and Schuurman [16] in a similar case, this differing symmetry affects the relative parity of the two nuclear WPs with respect to the coupling mode φ, thus making them nearly orthogonal. Specifically, the $\chi_{{}^3Q_0}$ WP is an even function showing a maximum around the equilibrium H—C—I bending angle, whereas the $\chi_{{}^1Q_1}$ WP, which is an odd function, has a minimum [see Fig. 1(b) and the WP evolutions provided in the WP movie reported in Supplemental Material [38]). The strict symmetries of the WPs, however, are broken by the introduction of a totally symmetric coupling element between the E and A_1 states due to the spin-orbit coupling (SOC) [75]. Therefore, the SOC prevents the WP overlap $\langle\chi_{{}^3Q_0}(t)|\chi_{{}^1Q_1}(t)\rangle$ from vanishing completely, but its weakness also explains the small magnitude of the predicted vibronic coherence. Interestingly, by leveraging the interference with the intense FWM_1 signal, even such a weak coherence is brought toward reasonable detection limits. As a demonstration of the sensitivity of the technique, Fig. 3(b) benchmarks the total FWM intensity [i.e., I_T in Eq. (1)] against the LO background obtained by blocking the VIS pulse [I_{LO} in Eq. (1)]. In particular, the FWM interference-fringe contrast is around 20% of the LO intensity. This represents a clear advantage of the heterodyne approach over homodyne detected FWM and conventional transient-absorption spectroscopy, neither of which benefit from such an improved sensitivity and unambiguous signal relation to electronic coherences.

One major insight from the simulated coherence presented in Fig. 3 is that, surprisingly, the coherence spawned at the molecular CI does not dephase completely when the iodine atom is fully dissociated from the rest of the molecule. Instead, Figs. 3(c) and 3(d) show that for $T >$ 80 fs the electronic coherence exhibits a constant oscillation with a 4.4 fs periodicity. This value corresponds to the spin-orbit splitting between the $j = \{1/2, 3/2\}$ states of iodine of $E_{\mathrm{SO}} = 0.94$ eV [76], suggesting that the original ${}^1Q_1 - {}^3Q_0$ electronic coherence, generated in the molecule, is observed at the atomic I fragment.

To further elucidate the evolution of the molecular complex coherence to the atomic regime we visualize its magnitude and phase in the Euler representation (see Fig. 4). Here, the initial coherence magnitude converges to a constant value (about 1/3 of its maximum) for $T > 80$ fs, while the coherence phase converges to a constant slope. This is expected in the atomic limit where nuclear motion does not influence the electronic coherence and no vibrational dephasing can occur. The CH_3I photodissociation time of about 80 fs, extrapolated with this analysis, agrees with reported experimental values [77]. The transition from the molecular to the atomic regime starts at 40 fs when the WPs travel away from the CI region. Because of the steeper slope of the ${}^1Q_1$ compared to the ${}^3Q_0$ PES, the centroid of the $\chi_{{}^1Q_1}$ WP moves faster along R than the $\chi_{{}^3Q_0}$ WP. These different velocities are compensated by the broadening of the two WPs, surprisingly leading to a

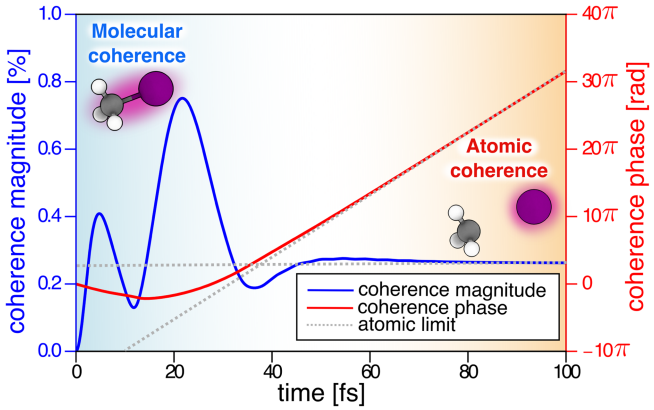

FIG. 4. Evolution of molecular coherence to the atomic regime. For early times after UV excitation (< 40 fs), the vibronic coherence magnitude (blue) shows large time-dependent modulations, while it converges to a constant value for later times (> 80 fs). The coherence phase (red) converges to a linear evolution for these later times. This convergence of the coherence magnitude and phase is a consequence of transitioning from a molecular to a dissociated atomic regime.

constant WP overlap and preventing a complete dephasing of the molecular coherence upon dissociation.

The fast oscillations in the atomic limit impose high temporal resolution requirements on the experiment. First, actinic photoexcitation will be achieved with sub-5-fs UV pulses [29,78–81] clearly separating the photoexcitation regime from WP propagation through the CI. Second, the Hd-FWM signal occurs after passage through the CI ($T > 15$ fs; see Fig. 3) and hence, the instrument response function out of temporal overlap with the actinic UV pulse is decisive. While the NIR (e.g., $\tau_{\mathrm{NIR}} < 5$ fs [82–84]) and VIS pulses (e.g., $\tau_{\mathrm{VIS}} < 25$ fs [85–87]) are of femtosecond duration, the isolated attosecond XUV pulse [71,88,89] acts as a temporal gate via core-level excitation. These laser pulse sources are readily available in many labs worldwide and lead to a subfemtosecond Hd-FWM instrument response function rise time (more details are given in Supplemental Material Sec. V [38]). They further typically provide a pulse-intensity stability of <0.5% for the NIR [90,91] and the VIS pulses [86] as well as a CEP stability of <200 mrad [92]. The Hd-FWM signal, however, is barely affected by such noise (see Supplemental Material Sec. VI [38]). Because of the heterodyned FWM scheme, only intensity and relative CEP fluctuations of the NIR_2 and the VIS pulses contribute to any potential reduction in the contrast of the Hd-FWM interference signal, while noise in the XUV and the NIR_1 pulses cancels out.

In summary, we show that one-third of the maximum vibronic coherence generated in photoexcited CH_3I by a CI remains as electronic coherence in the atomic iodine fragments after dissociation. This allows one to measure coherences spawned at CIs even when the pump-probe measurement delay is long after the WP propagation through the CI. To measure the evolution of the respective coherence between ${}^3Q_0$ and ${}^1Q_1$ electronic states, we present the heterodyned attosecond FWM spectroscopic technique. Here, two FWM signals that originate from mixing an attosecond XUV pulse with two NIR pulses or with one NIR and one VIS pulse, respectively, can be interfered with each other. The Hd-FWM signal directly maps the temporal evolution of the vibronic coherence with high sensitivity and subfemtosecond resolution. Moreover, it allows one to trace the full complex coherence function by cycling the relative CEP between one NIR and the VIS pulse and, therefore, enabling a quantum-state tomography. The Hd-FWM technique as discussed in this Letter is based on realistic tabletop experimental parameters and is, hence, relevant and accessible for the ultrafast scientific community.

This Letter frontiers the idea of using photochemistry to prepare long-lived electronic coherence in atoms after molecular dissociation. Hd-FWM as a core-level spectroscopic technique benefits from atomic site specificity and sensitivity to the intramolecular chemical environment [93]. Hence, Hd-FWM will grant insights into the coherence dynamics of complex photochemically active molecules. As this approach avoids decoherence effects in molecules, it results in robust coherent states of gas-phase atoms and, hence, constitutes a potential building block for ultrafast quantum information technology [94–98]. The only remaining potential decoherence mechanism is from particle collisions. Because of the utilized dilute gas sample, however, the expected average collision time is in the nanosecond regime, which is several orders of magnitude slower than typical vibrationally induced dephasing (tens to hundreds of femtoseconds). In the future, Hd-FWM will enable studies targeting coherent control of molecular coherence, e.g., with shaped UV pulses. Moreover, this Letter adds to the toolbox of coherent-control of spin-orbit effects [99].

Acknowledgments—We thank Jérémy R. Rouxel, Wolfgang Domcke, and Lea Maria Ibele for valuable discussions. This Letter was performed by personnel and equipment supported by the Office of Science, Office of Basic Energy Sciences through the Atomic, Molecular, and Optical Sciences Program of the Division of Chemical Sciences, Geosciences, and Biosciences of the U.S. Department of Energy (DOE) at Lawrence Berkeley National Laboratory under Contracts No. DE-AC02-05CH11231 (P. R., N. G. P., D. M. N., and S. R. L.) and No. DE-SC0022225 [S. M. at the University of California, Irvine; F. M. and M. G. at the University of Bologna, Italy; L. X. and N. G. under FWP 72684 at the Pacific Northwest National Laboratory (PNNL)]. P. R. acknowledges funding by the Alexander von Humboldt Foundation (Feodor Lynen Fellowship). N. G. P. acknowledges funding from Soroptimist International of the Americas (Founder Region

Fellowship). This work was also supported by ERC grant QuantXS, No. 101116417. The research benefited from computational resources provided by PNNL's Institutional Computing (PIC) Program, Environmental Molecular Sciences Laboratory (EMSL), a DOE Office of Science User Facility sponsored by the Office of Biological and Environmental Research and located at PNNL, and the National Energy Research Scientific Computing Center (NERSC), a U.S. Department of Energy Office of Science User Facility operated under Contract No. DE-AC02-05CH11231. PNNL is operated by Battelle Memorial Institute for the United States Department of Energy under DOE Contract No. DE-AC05-76RL1830.

P. R. and F. M. contributed equally to this work. P. R. and S. R. L. conceptualized the project. P. R., N. G. P., D. M. N., and S. R. L. developed the Hd-FWM scheme. F. M. and D. K. conceptualized the response theory. L. X. and N. G. conducted the quantum chemistry calculations. F. M. and D. K. conducted the Hd-FWM simulation with input from S. M. and M. G.. The work was supervised by N. G., M. G., D. M. N., S. R. L., and D. K.. P. R. and F. M. wrote the manuscript with input from all authors.

Data availability—The data that support the findings of this Letter are openly available [37].

[1] A. Streltsov, G. Adesso, and M. B. Plenio, Colloquium: Quantum coherence as a resource, Rev. Mod. Phys. **89**, 041003 (2017).
[2] J. D. Schultz, J. L. Yuly, E. A. Arsenault, K. Parker, S. N. Chowdhury, R. Dani, S. Kundu, H. Nuomin, Z. Zhang, J. Valdiviezo, P. Zhang, K. Orcutt, S. J. Jang, G. R. Fleming, N. Makri, J. P. Ogilvie, M. J. Therien, M. R. Wasielewski, and D. N. Beratan, Coherence in chemistry: Foundations and frontiers, Chem. Rev. **124**, 11641 (2024).
[3] Z. Xi, Y. Li, and H. Fan, Quantum coherence and correlations in quantum system, Sci. Rep. **5**, 10922 (2015).
[4] H. Timmers, X. Zhu, Z. Li, Y. Kobayashi, M. Sabbar, M. Hollstein, M. Reduzzi, T. J. Martínez, D. M. Neumark, and S. R. Leone, Disentangling conical intersection and coherent molecular dynamics in methyl bromide with attosecond transient absorption spectroscopy, Nat. Commun. **10**, 3133 (2019).
[5] N. Saito, H. Sannohe, N. Ishii, T. Kanai, N. Kosugi, Y. Wu, A. Chew, S. Han, Z. Chang, and J. Itatani, Real-time observation of electronic, vibrational, and rotational dynamics in nitric oxide with attosecond soft x-ray pulses at 400 eV, Optica **6**, 1542 (2019).
[6] Y. Kobayashi and S. R. Leone, Characterizing coherences in chemical dynamics with attosecond time-resolved x-ray absorption spectroscopy, J. Chem. Phys. **157**, 180901 (2022).
[7] M. Kowalewski, B. P. Fingerhut, K. E. Dorfman, K. Bennett, and S. Mukamel, Simulating coherent multidimensional spectroscopy of nonadiabatic molecular processes: From the infrared to the x-ray regime, Chem. Rev. **117**, 12165 (2017).
[8] W. Domcke, D. Yarkony, and H. Köppel, *Conical Intersections: Electronic Structure, Dynamics & Spectroscopy* (World Scientific, Singapore, 2004), Vol. 15.
[9] T. Schultz, E. Samoylova, W. Radloff, I. V. Hertel, A. L. Sobolewski, and W. Domcke, Efficient deactivation of a model base pair via excited-state hydrogen transfer, Science **306**, 1765 (2004).
[10] D. Polli, P. Altoè, O. Weingart, K. M. Spillane, C. Manzoni, D. Brida, G. Tomasello, G. Orlandi, P. Kukura, R. A. Mathies *et al.*, Conical intersection dynamics of the primary photoisomerization event in vision, Nature (London) **467**, 440 (2010).
[11] V. Tiwari, W. K. Peters, and D. M. Jonas, Electronic resonance with anticorrelated pigment vibrations drives photosynthetic energy transfer outside the adiabatic framework, Proc. Natl. Acad. Sci. U.S.A. **110**, 1203 (2013).
[12] W. J. Schreier, P. Gilch, and W. Zinth, Early events of DNA photodamage, Annu. Rev. Phys. Chem. **66**, 497 (2015).
[13] A. J. Musser, M. Liebel, C. Schnedermann, T. Wende, T. B. Kehoe, A. Rao, and P. Kukura, Evidence for conical intersection dynamics mediating ultrafast singlet exciton fission, Nat. Phys. **11**, 352 (2015).
[14] M. S. Schuurman and A. Stolow, Dynamics at conical intersections, Annu. Rev. Phys. Chem. **69**, 427 (2018).
[15] T. J. Wolf, D. M. Sanchez, J. Yang, R. Parrish, J. Nunes, M. Centurion, R. Coffee, J. Cryan, M. Gühr, K. Hegazy *et al.*, The photochemical ring-opening of 1,3-cyclohexadiene imaged by ultrafast electron diffraction, Nat. Chem. **11**, 504 (2019).
[16] S. P. Neville, A. Stolow, and M. S. Schuurman, Formation of electronic coherences in conical intersection-mediated dynamics, J. Phys. B **55**, 044004 (2022).
[17] S. M. Cavaletto, Y. Nam, J. R. Rouxel, D. Keefer, H. Yong, and S. Mukamel, Attosecond monitoring of nonadiabatic molecular dynamics by transient x-ray transmission spectroscopy, J. Chem. Theory Comput. **19**, 2327 (2023).
[18] K. Bennett, M. Kowalewski, J. R. Rouxel, and S. Mukamel, Monitoring molecular nonadiabatic dynamics with femtosecond x-ray diffraction, Proc. Natl. Acad. Sci. U.S.A. **115**, 6538 (2018).
[19] J. R. Rouxel, D. Keefer, and S. Mukamel, Signatures of electronic and nuclear coherences in ultrafast molecular x-ray and electron diffraction, Struct. Dyn. **8**, 014101 (2021).
[20] M. Kowalewski, K. Bennett, K. E. Dorfman, and S. Mukamel, Catching conical intersections in the act: Monitoring transient electronic coherences by attosecond stimulated x-ray Raman signals, Phys. Rev. Lett. **115**, 193003 (2015).
[21] B. W. McNeil and N. R. Thompson, X-ray free-electron lasers, Nat. Photonics **4**, 814 (2010).
[22] S. Weathersby, G. Brown, M. Centurion, T. Chase, R. Coffee, J. Corbett, J. Eichner, J. Frisch, A. Fry, M. Gühr *et al.*, Mega-electron-volt ultrafast electron diffraction at SLAC national accelerator laboratory, Rev. Sci. Instrum. **86**, 073702 (2015).
[23] D. Imre, J. L. Kinsey, A. Sinha, and J. Krenos, Chemical dynamics studied by emission spectroscopy of dissociating molecules, J. Phys. Chem. **88**, 3956 (1984).

[24] D. Zhong and A. H. Zewail, Femtosecond real-time probing of reactions. 23. Studies of temporal, velocity, angular, and state dynamics from transition states to final products by femtosecond-resolved mass spectrometry, J. Chem. Phys. A **102**, 4031 (1998).
[25] R. de Nalda, J. Durá, A. García-Vela, J. G. Izquierdo, J. González-Vázquez, and L. Bañares, A detailed experimental and theoretical study of the femtosecond A-band photodissociation of CH_3I, J. Chem. Phys. **128**, 244309 (2008).
[26] A. R. Attar, A. Bhattacherjee, and S. R. Leone, Direct observation of the transition-state region in the photodissociation of CH_3I by femtosecond extreme ultraviolet transient absorption spectroscopy, J. Phys. Chem. Lett. **6**, 5072 (2015).
[27] L. Drescher, M. Galbraith, G. Reitsma, J. Dura, N. Zhavoronkov, S. Patchkovskii, M. Vrakking, and J. Mikosch, Communication: XUV transient absorption spectroscopy of iodomethane and iodobenzene photodissociation, J. Chem. Phys. **145**, 011101 (2016).
[28] K. F. Chang, H. Wang, S. M. Poullain, D. Prendergast, D. M. Neumark, and S. R. Leone, Mapping wave packet bifurcation at a conical intersection in CH_3I by attosecond XUV transient absorption spectroscopy, J. Chem. Phys. **154**, 251106 (2021).
[29] L. Colaizzi, S. Ryabchuk, E. P. Månsson, K. Saraswathula, V. Wanie, A. Trabattoni, J. González-Vázquez, F. Martín, and F. Calegari, Few-femtosecond time-resolved study of the UV-induced dissociative dynamics of iodomethane, Nat. Commun. **15**, 9196 (2024).
[30] Y. Amatatsu, S. Yabushita, and K. Morokuma, Full nine-dimensional ab-initio potential energy surfaces and trajectory studies of A-band photodissociation dynamics: $CH_3I^* \rightarrow CH_3 + I$, $CH_3 + I^*$, and $CD_3I^* \rightarrow CD_3 + I$, $CD_3 + I^*$, J. Chem. Phys. **104**, 9783 (1996).
[31] D. Xie, H. Guo, Y. Amatatsu, and R. Kosloff, Three-dimensional photodissociation dynamics of rotational state selected methyl iodide, J. Chem. Phys. A **104**, 1009 (2000).
[32] C. R. Evenhuis and U. Manthe, Photodissociation of CH_3I: A full-dimensional (9D) quantum dynamics study, J. Chem. Phys. A **115**, 5992 (2011).
[33] H. Wang, M. Odelius, and D. Prendergast, A combined multi-reference pump-probe simulation method with application to XUV signatures of ultrafast methyl iodide photodissociation, J. Chem. Phys. **151**, 124106 (2019).
[34] C. M. Roehl, J. B. Burkholder, G. K. Moortgat, A. Ravishankara, and P. J. Crutzen, Temperature dependence of UV absorption cross sections and atmospheric implications of several alkyl iodides, J. Geophys. Res.-Atmos. **102**, 12819 (1997).
[35] A. T. Eppink and D. Parker, Energy partitioning following photodissociation of methyl iodide in the A band: A velocity mapping study, J. Chem. Phys. **110**, 832 (1999).
[36] M. Kowalewski and R. de Vivie-Riedle, QDng: A grid based molecular quantum dynamics package, Zenodo, 10.5281/zenodo.10944496 (2024).
[37] P. Rupprecht, F. Montorsi, X. Lei, N. G. Puskar, M. Garavelli, S. Mukamel, N. Govind, D. M. Neumark, D. Keefer, and S. R. Leone, Source data of: Tracing long-lived atomic coherences generated via molecular conical intersections, Zenodo, 10.5281/zenodo.16745467 (2025).
[38] See Supplemental Material at http://link.aps.org/supplemental/10.1103/6bfk-mgpn for further information on the effective Hamiltonian, the wave-packet propagation, the electronic structure theory, and the derivation of the Hd-FWM signal, as well as the instrument response function and laser-pulse noise considerations, which includes Refs. [39–53].
[39] P. H. Berens and K. R. Wilson, Molecular dynamics and spectra. I. Diatomic rotation and vibration, J. Chem. Phys. **74**, 4872 (1981).
[40] H. Tal-Ezer and R. Kosloff, An accurate and efficient scheme for propagating the time dependent Schrödinger equation, J. Chem. Phys. **81**, 3967 (1984).
[41] G. A. Fiete and E. J. Heller, Semiclassical theory of coherence and decoherence, Phys. Rev. A **68**, 022112 (2003).
[42] M. Vacher, M. J. Bearpark, M. A. Robb, and J. P. Malhado, Electron dynamics upon ionization of polyatomic molecules: Coupling to quantum nuclear motion and decoherence, Phys. Rev. Lett. **118**, 083001 (2017).
[43] K. F. Chang, H. Wang, S. M. Poullain, J. González-Vázquez, L. Bañares, D. Prendergast, D. M. Neumark, and S. R. Leone, Conical intersection and coherent vibrational dynamics in alkyl iodides captured by attosecond transient absorption spectroscopy, J. Chem. Phys. **156**, 114304 (2022).
[44] J. G. Hill and K. A. Peterson, Correlation consistent basis sets for explicitly correlated wavefunctions: Pseudopotential–based basis sets for the post–d main group elements Ga–Rn, J. Chem. Phys. **141**, 094106 (2014).
[45] T. H. Dunning Jr., Gaussian basis sets for use in correlated molecular calculations. I. The atoms boron through neon and hydrogen, J. Chem. Phys. **90**, 1007 (1989).
[46] P. O. Widmark, P. Å. Malmqvist, and B. O. Roos, Density matrix averaged atomic natural orbital (ANO) basis sets for correlated molecular wave functions I. First row atoms, Theor. Chim. Acta **77**, 291 (1990).
[47] T. Helgaker, P. Jørgensen, and J. Olsen, *Molecular Electronic-Structure Theory* (Wiley, Chichester, 2000).
[48] A. Berning, M. Schweizer, H.-J. Werner, P. J. Knowles, and P. Palmieri, Spin-orbit matrix elements for internally contracted multireference configuration interaction wavefunctions, Mol. Phys. **98**, 1823 (2000).
[49] A. Mitrushchenkov and H.-J. Werner, Calculation of transition moments between internally contracted MRCI wave functions with non-orthogonal orbitals, Mol. Phys. **105**, 1239 (2007).
[50] L. Nahon, P. Morin, and F. C. Farnoux, Relaxation of the $nd \rightarrow (n+1)p$ resonances in atomic bromine and iodine, Phys. Scr. **1992**, 104 (1992).
[51] M. Chini, H. Mashiko, H. Wang, S. Chen, C. Yun, S. Scott, S. Gilbertson, and Z. Chang, Delay control in attosecond pump-probe experiments, Opt. Express **17**, 21459 (2009).
[52] M. Huppert, I. Jordan, and H. J. Wörner, Attosecond beamline with actively stabilized and spatially separated beam paths, Rev. Sci. Instrum. **86**, 123106 (2015).
[53] F. Schlaepfer, M. Volkov, N. Hartmann, A. Niedermayr, Z. Schumacher, L. Gallmann, and U. Keller, Phase stabilization of an attosecond beamline combining two IR colors, Opt. Express **27**, 22385 (2019).

[54] G. O'Sullivan, The absorption spectrum of CH_3I in the extreme VUV, J. Phys. B: At. Mol. Opt. Phys. **15**, L327 (1982).

[55] H. Werner and P. J. Knowles, An efficient internally contracted multiconfiguration—reference configuration interaction method, J. Chem. Phys. **89**, 5803 (1988).

[56] P. J. Knowles and H. J. Werner, Internally contracted multiconfiguration—reference configuration interaction calculations for excited states, Theor. Chim. Acta **84**, 95 (1992).

[57] H. J. Werner, P. J. Knowles, G. Knizia, F. R. Manby, and M. Schütz, MOLPRO: A general-purpose quantum chemistry program package, Wiley Rev: Comp. Mol. Sci. **2**, 242 (2012).

[58] W. Cao, E. R. Warrick, A. Fidler, D. M. Neumark, and S. R. Leone, Noncollinear wave mixing of attosecond XUV and few-cycle optical laser pulses in gas-phase atoms: Toward multidimensional spectroscopy involving XUV excitations, Phys. Rev. A **94**, 053846 (2016).

[59] A. P. Fidler, S. J. Camp, E. R. Warrick, E. Bloch, H. J. Marroux, D. M. Neumark, K. J. Schafer, M. B. Gaarde, and S. R. Leone, Nonlinear XUV signal generation probed by transient grating spectroscopy with attosecond pulses, Nat. Commun. **10**, 1384 (2019).

[60] H. J. Marroux, A. P. Fidler, D. M. Neumark, and S. R. Leone, Multidimensional spectroscopy with attosecond extreme ultraviolet and shaped near-infrared pulses, Sci. Adv. **4**, eaau3783 (2018).

[61] A. P. Fidler, H. J. Marroux, E. R. Warrick, E. Bloch, W. Cao, S. R. Leone, and D. M. Neumark, Autoionization dynamics of $(^2P_{1/2})ns/d$ states in krypton probed by noncollinear wave mixing with attosecond extreme ultraviolet and few-cycle near infrared pulses, J. Chem. Phys. **151**, 114305 (2019).

[62] N. G. Puskar, Y.-C. Lin, J. D. Gaynor, M. C. Schuchter, S. Chattopadhyay, C. Marante, A. P. Fidler, C. L. Keenan, L. Argenti, D. M. Neumark *et al.*, Measuring autoionization decay lifetimes of optically forbidden inner valence excited states in neon atoms with attosecond noncollinear four-wave-mixing spectroscopy, Phys. Rev. A **107**, 033117 (2023).

[63] J. D. Gaynor, A. P. Fidler, Y. Kobayashi, Y.-C. Lin, C. L. Keenan, D. M. Neumark, and S. R. Leone, Nonresonant coherent amplitude transfer in attosecond four-wave-mixing spectroscopy, Phys. Rev. A **107**, 023526 (2023).

[64] P. Rupprecht, N. G. Puskar, D. M. Neumark, and S. R. Leone, Extracting doubly excited state lifetimes in helium directly in the time domain with attosecond noncollinear four-wave-mixing spectroscopy, Phys. Rev. Res. **6**, 043100 (2024).

[65] W. Cao, E. R. Warrick, A. Fidler, S. R. Leone, and D. M. Neumark, Excited-state vibronic wave-packet dynamics in H_2 probed by XUV transient four-wave mixing, Phys. Rev. A **97**, 023401 (2018).

[66] Y.-C. Lin, A. P. Fidler, A. Sandhu, R. R. Lucchese, C. W. McCurdy, S. R. Leone, and D. M. Neumark, Coupled nuclear–electronic decay dynamics of O_2 inner valence excited states revealed by attosecond XUV wave-mixing spectroscopy, Faraday Discuss. **228**, 537 (2021).

[67] A. P. Fidler, Y.-C. Lin, J. D. Gaynor, C. W. McCurdy, S. R. Leone, R. R. Lucchese, and D. M. Neumark, State-selective probing of CO_2 autoionizing inner valence Rydberg states with attosecond extreme ultraviolet four-wave-mixing spectroscopy, Phys. Rev. A **106**, 063525 (2022).

[68] J. D. Gaynor, A. P. Fidler, Y.-C. Lin, H.-T. Chang, M. Zuerch, D. M. Neumark, and S. R. Leone, Solid state core-exciton dynamics in NaCl observed by tabletop attosecond four-wave mixing spectroscopy, Phys. Rev. B **103**, 245140 (2021).

[69] P. B. Corkum, Plasma perspective on strong field multiphoton ionization, Phys. Rev. Lett. **71**, 1994 (1993).

[70] K. Schafer, B. Yang, L. DiMauro, and K. Kulander, Above threshold ionization beyond the high harmonic cutoff, Phys. Rev. Lett. **70**, 1599 (1993).

[71] F. Krausz and M. Ivanov, Attosecond physics, Rev. Mod. Phys. **81**, 163 (2009).

[72] W. Cao, E. R. Warrick, A. Fidler, S. R. Leone, and D. M. Neumark, Near-resonant four-wave mixing of attosecond extreme-ultraviolet pulses with near-infrared pulses in neon: Detection of electronic coherences, Phys. Rev. A **94**, 021802 (2016).

[73] S. Mukamel, *Principles of Nonlinear Optical Spectroscopy* (Oxford University Press, New York, 1995).

[74] P. Tian, D. Keusters, Y. Suzaki, and W. S. Warren, Femtosecond phase-coherent two-dimensional spectroscopy, Science **300**, 1553 (2003).

[75] S. Bhattacharyya, D. Opalka, L. V. Poluyanov, and W. Domcke, The $(\mathrm{E}+\mathrm{A})\times(\mathrm{e}+\mathrm{a})$ Jahn–Teller and pseudo-Jahn–Teller Hamiltonian including spin–orbit coupling for trigonal systems, J. Phys. Chem. A **118**, 11962 (2014).

[76] G. O'Sullivan, C. McGuinness, J. T. Costello, E. T. Kennedy, and B. Weinmann, Trends in 4d-subshell photoabsorption along the iodine isonuclear sequence: I, I^+, and I^{2+}, Phys. Rev. A **53**, 3211 (1996).

[77] M. E. Corrales, V. Loriot, G. Balerdi, J. González-Vázquez, R. de Nalda, L. Banares, and A. H. Zewail, Structural dynamics effects on the ultrafast chemical bond cleavage of a photodissociation reaction, Phys. Chem. Chem. Phys. **16**, 8812 (2014).

[78] U. Graf, M. Fieß, M. Schultze, R. Kienberger, F. Krausz, and E. Goulielmakis, Intense few-cycle light pulses in the deep ultraviolet, Opt. Express **16**, 18956 (2008).

[79] M. Galli, V. Wanie, D. P. Lopes, E. P. Månsson, A. Trabattoni, L. Colaizzi, K. Saraswathula, A. Cartella, F. Frassetto, L. Poletto *et al.*, Generation of deep ultraviolet sub-2-fs pulses, Opt. Lett. **44**, 1308 (2019).

[80] J. C. Travers, T. F. Grigorova, C. Brahms, and F. Belli, High-energy pulse self-compression and ultraviolet generation through soliton dynamics in hollow capillary fibres, Nat. Photonics **13**, 547 (2019).

[81] M. Reduzzi, M. Pini, L. Mai, F. Cappenberg, L. Colaizzi, F. Vismarra, A. Crego, M. Lucchini, C. Brahms, J. Travers *et al.*, Direct temporal characterization of sub-3-fs deep UV pulses generated by resonant dispersive wave emission, Opt. Express **31**, 26854 (2023).

[82] A. L. Cavalieri, E. Goulielmakis, B. Horvath, W. Helml, M. Schultze, M. Fieß, V. Pervak, L. Veisz, V. Yakovlev, M. Uiberacker *et al.*, Intense 1.5-cycle near infrared laser waveforms and their use for the generation of ultra-broadband soft-x-ray harmonic continua, New J. Phys. **9**, 242 (2007).

[83] H. Timmers, Y. Kobayashi, K. F. Chang, M. Reduzzi, D. M. Neumark, and S. R. Leone, Generating high-contrast, near single-cycle waveforms with third-order dispersion compensation, Opt. Lett. **42**, 811 (2017).
[84] T. Nagy, P. Simon, and L. Veisz, High-energy few-cycle pulses: Post-compression techniques, Adv. Phys.-X **6**, 1845795 (2021).
[85] J. Liu, Y. Kida, T. Teramoto, and T. Kobayashi, Generation of stable sub-10 fs pulses at 400 nm in a hollow fiber for UV pump-probe experiment, Opt. Express **18**, 4664 (2010).
[86] F. Hu, Z. Wang, Q. Yao, W. Cao, Q. Zhang, and P. Lu, Clean hundred-μJ-level sub-6-fs blue pulses generated with helium-assisted solid thin plates, Opt. Lett. **48**, 2555 (2023).
[87] J.-H. Ou, D. Hait, P. Rupprecht, J. E. Beetar, T. J. Martínez, and S. R. Leone, Attosecond probing of coherent vibrational dynamics in CBr_4, J. Phys. Chem. A **128**, 9208 (2024).
[88] M. Hentschel, R. Kienberger, C. Spielmann, G. A. Reider, N. Milosevic, T. Brabec, P. Corkum, U. Heinzmann, M. Drescher, and F. Krausz, Attosecond metrology, Nature (London) **414**, 509 (2001).
[89] M. Chini, K. Zhao, and Z. Chang, The generation, characterization and applications of broadband isolated attosecond pulses, Nat. Photonics **8**, 178 (2014).
[90] https://www.coherent.com/content/dam/coherent/site/en/resources/datasheet/lasers/astrella-ds.pdf, stability specifications of a typical state-of-the-art Titanium:Sapphire laser system (Coherent Inc. Astrella).
[91] P. D. Rupprecht, Ultrafast laser control of molecular quantum dynamics from a core-electron perspective, Ph.D. thesis, Ruperto-Carola-University of Heidelberg, 2022.
[92] M. Musheghyan, F. Lücking, Z. Cheng, H. Frei, and A. Assion, 0.24 TW ultrabroadband, CEP-stable multipass Ti:Sa amplifier, Opt. Lett. **44**, 1464 (2019).
[93] K. Siegbahn, Electron spectroscopy for atoms, molecules, and condensed matter, Rev. Mod. Phys. **54**, 709 (1982).
[94] R. de Vivie-Riedle and U. Troppmann, Femtosecond lasers for quantum information technology, Chem. Rev. **107**, 5082 (2007).
[95] J. G. Underwood, M. Spanner, M. Y. Ivanov, J. Mottershead, B. J. Sussman, and A. Stolow, Switched wave packets: A route to nonperturbative quantum control, Phys. Rev. Lett. **90**, 223001 (2003).
[96] L.-M. Koll, L. Maikowski, L. Drescher, T. Witting, and M. J. Vrakking, Experimental control of quantum-mechanical entanglement in an attosecond pump-probe experiment, Phys. Rev. Lett. **128**, 043201 (2022).
[97] F. Shobeiry, P. Fross, H. Srinivas, T. Pfeifer, R. Moshammer, and A. Harth, Emission control of entangled electrons in photoionisation of a hydrogen molecule, Sci. Rep. **14**, 19630 (2024).
[98] F. Bouchard, K. Fenwick, K. Bonsma-Fisher, D. England, P. J. Bustard, K. Heshami, and B. Sussman, Programmable photonic quantum circuits with ultrafast time-bin encoding, Phys. Rev. Lett. **133**, 090601 (2024).
[99] P. Rupprecht, L. Aufleger, S. Heinze, A. Magunia, T. Ding, M. Rebholz, S. Amberg, N. Mollov, F. Henrich, M. W. Haverkort *et al.*, Laser control of electronic exchange interaction within a molecule, Phys. Rev. Lett. **128**, 153001 (2022).